

Water adsorption isotherms on porous onionlike carbonaceous particles. Simulations with the grand canonical Monte Carlo method

György Hantal,^{1,2} Sylvain Picaud,^{2,a)} Paul N. M. Hoang,² Vladimir P. Voloshin,³ Nikolai N. Medvedev,³ and Pál Jedlovsky^{1,4,b)}

¹Laboratory of Interfaces and Nanosized Systems, Institute of Chemistry, Eötvös Loránd University, Pázmány Péter stny. 1/a, H-1117 Budapest, Hungary

²Institut UTINAM, UMR 6213 CNRS/Université de Franche-Comté, F-25030 Besançon Cedex, France

³Group of Supramolecular Structures, Institute of Chemical Kinetics and Combustion, Siberian Branch of the RAS, Institutskaya 3, R-630090 Novosibirsk, Russia

⁴HAS Research Group of Technical Analytical Chemistry, Szt. Gellért tér 4, H-1111 Budapest, Hungary and EKF Department of Chemistry, Leányka u. 6, H-3300 Eger, Hungary

(Received 4 June 2010; accepted 13 September 2010; published online 8 October 2010)

The grand canonical Monte Carlo method is used to simulate the adsorption isotherms of water molecules on different types of model soot particles. These soot models are constructed by first removing atoms from onion-fullerene structures in order to create randomly distributed pores inside the soot, and then performing molecular dynamics simulations, based on the reactive adaptive intermolecular reactive empirical bond order (AIREBO) description of the interaction between carbon atoms, to optimize the resulting structures. The obtained results clearly show that the main driving force of water adsorption on soot is the possibility of the formation of new water-water hydrogen bonds with the already adsorbed water molecules. The shape of the calculated water adsorption isotherms at 298 K strongly depends on the possible confinement of the water molecules in pores of the carbonaceous structure. We found that there are two important factors influencing the adsorption ability of soot. The first of these factors, dominating at low pressures, is the ability of the soot of accommodating the first adsorbed water molecules at strongly hydrophilic sites. The second factor concerns the size and shape of the pores, which should be such that the hydrogen bonding network of the water molecules filling them should be optimal. This second factor determines the adsorption properties at higher pressures. © 2010 American Institute of Physics.

[doi:10.1063/1.3496466]

I. INTRODUCTION

Soot produced by aircraft is suspected to have a non-negligible influence on atmospheric chemistry and on greenhouse effect.¹ Indeed, aircraft-generated soot is directly emitted in the upper troposphere-lower stratosphere (UTLS) region, where it allows heterogeneous ice nucleation resulting in the formation of condensation trails behind planes.² These contrails may evolve into artificial cirrus clouds, which thus add their effect on climate to natural clouds^{3–5} with a balance between reflecting solar radiations and absorbing terrestrial radiation, a process that is not yet precisely quantified.⁶

Moreover, the formation of soot and of ice particles nucleated around soot provides solid surfaces in the UTLS for adsorption and subsequent heterogeneous reactions, which are suspected to modify the composition of the gas phase. For instance, polycyclic aromatic hydrocarbons may likely interact with carbonaceous particles constituting soot, which thus may act as a sink for this class of atmospheric compounds.^{7–9} In a similar way, selective adsorption of volatile organic compounds (VOCs) on ice particles may influence the gas phase partition in the UTLS, and modify the

fate of these VOCs in the atmosphere.¹⁰ However, a quantitative study of the impact of soot on atmosphere and climate is a challenging task because it requires geometrical, chemical, and optical characterization of the primary carbonaceous particles constituting soot.¹¹ As a consequence, and because *in situ* measurements are hardly feasible, the hydration properties of soot in real conditions, e.g., behind airplanes are still poorly known.

Recent transmission electron microscopy studies have shown that soot emitted by aircraft is made of nanocrystallites containing graphite-type layers arranged in an onionlike structure. Soot particles are thus of quasispherical shape, with diameters ranging between 5 and 50 nm.^{12,13} Results of recent Raman spectroscopy measurements have confirmed that these graphite layers are partially oxidized, and they contain a certain number of hydrophilic sites.¹⁴ The presence of both such polar groups and micropores in the structure of the soot can explain the unexpected affinity between such carbonaceous particles and water.¹⁵ Indeed, although soot is expected to be nonwetttable in the initial stages of its formation,¹⁶ a few experiments including measurements of water adsorption isotherms at room temperature have shown that aircraft soot, like *n*-hexane soot, flame soot, or carbonaceous particles may become partially hydrated due to the presence of functional groups that can form hydrogen bonds

^{a)}Electronic mail: sylvain.picaud@univ-fcomte.fr.

^{b)}Electronic mail: pali@chem.elte.hu.

with water molecules.^{15,17–21} The emerging picture from these studies is that surface adsorption, increasing with the number of oxidized surface groups, is the dominant process at low relative humidities. At higher relative humidities, further adsorption occurs in the micropores of the soot, followed finally by multilayer adsorption.^{19,22}

From a fundamental point of view, a detailed understanding of the water nucleation on spherical soot particles at the molecular level remains challenging, although a lot of theoretical studies have been recently published on the adsorption of water in porous carbon.^{23–28} Such a molecular level understanding can be achieved by performing either first-principles calculations, or numerical simulations based on empirical potentials to describe the water-soot interactions, or by the combination of both approaches.

In a series of previous papers, we used quantum mechanical calculations^{29–32} to characterize the influence of the polar OH, COOH, and C–O–C (epoxidelike) groups on water adsorption at a partially oxidized soot particle of nanometer size. The results of our calculations have clearly shown the preferential adsorption of water molecules at carbonaceous surfaces containing carboxyl rather than hydroxyl or epoxidelike groups because of the possible formation of two hydrogen bonds between the COOH group and the water molecules. These results have been confirmed by classical molecular dynamics simulations performed at finite temperature using empirical potential models fitted to results of quantum mechanical calculations.^{33–35} Furthermore, in understanding the reasons of water adsorption the influence of the specific, round-shape morphology of the soot nanoparticles on the adsorption of water has also to be taken into account. Therefore, in two recent papers^{36,37} we have used the grand canonical Monte Carlo (GCMC) method³⁸ to calculate water adsorption isotherms on model soot particles of spherical shape. These soot particles were either made of carbon atoms only,³⁶ or containing also a small amount of oxygen atoms in the form of COOH and OH groups randomly distributed inside the volume or/and at the surface of the particle.³⁷ The main conclusion of these works was that the driving force of the water adsorption outside or/and inside carbonaceous nanoparticles mostly comes from the attraction of the already adsorbed water molecules. Thus, water molecules can be trapped once few water molecules are already adsorbed, as these molecules can act as condensation nuclei for the additional water molecules. These first water molecules can be trapped by hydrophilic chemical groups, or by confinement effects in pores of small size. However, this latter conclusion might depend not only on the size of the pores, but also on the way they are created in the carbonaceous structure. Indeed, we used in the previous GCMC calculations soot nanoparticles made of randomly distributed elemental chemical units on concentric spheres, each elemental unit containing 19 C atoms arranged in five fused benzene rings.^{36,37} Such an arrangement leads to the formation of a very porous carbonaceous structure, which might be far from the real structure of stable soot nanoparticles.

In order to further investigate this problem, we perform here GCMC simulations to characterize the water adsorption on more realistic carbonaceous nanoparticles. Thus, the soot

models used in the present study are made by removing carbon atoms in well-optimized structures of onion-fullerenes. In this way, particles characterized by different densities of the C atoms and various distributions of pores of different shape and size are created. Then molecular dynamics simulation is employed to optimize the resulting structures using the adaptive intermolecular reactive empirical bond order (AIREBO) potential to describe the carbon-carbon interactions.³⁹ Besides the usual nonbonding interactions this potential can also describe the formation and breaking of C–C chemical bonds, as it is able to switch smoothly between the so-called second generation REBO potential⁴⁰ and a Lennard-Jones term depending on the relative distance between the interacting atoms. Further, this potential is known to realistically represent carbon-carbon interaction for various states of hybridization. The nanoparticles created this way are thus more realistic than the ones used in our previous studies in the sense that we now ensure the chemical stability of the structure at the temperature of the GCMC simulations.

II. COMPUTATIONAL DETAILS

A. Soot models

In the present study, two different types of soot particles have been considered. The starting point in the construction of type I particles has been a soot ball with an onionlike structure consisting of four concentric spherical fullerene molecules that can be characterized by the radii of 7.04 Å (C₂₄₀), 10.89 Å (C₅₄₀), 14.36 Å (C₉₆₀) and 18.15 Å (C₁₅₀₀). In this C₂₄₀@C₅₄₀@C₉₆₀@C₁₅₀₀ particle the distance between two successive shells ranges from 3.5 to 3.8 Å, close to the distance of two successive graphite layers.⁴¹ (It should be noted that this particle already contains a relatively large pore in its center, which, in principle, could incorporate an innermost C₆₀ fullerene.) Then, at the surface of each shell, pores of a radius varying from 1.2 to 3.4 Å have been created in randomly chosen positions. Two neighboring pores have been separated by the distance of 3.0–6.8 Å from each other. Four models of this type, consisting of 2976, 2376, 2207, and 2133 carbon atoms, respectively, have been generated with different pore densities. The resulting structures have then been relaxed in a molecular dynamics simulation, performed on the canonical (*N, V, T*) ensemble at 298 K, in which the C–C interactions have been described using the reactive AIREBO potential.³⁹ These simulations have been 48 ps long, using the integration time step of 1 fs. This procedure has resulted in four different soot models, characterized by different carbon atom densities and morphologically different cavities. The particles containing 2976, 2376, 2207, and 2133 carbon atoms, shown in Figure 1, are referred to here from now on as *S*₁^I, *S*₂^I, *S*₃^I, and *S*₄^I, respectively.

A different type of soot particle, marked as type II, has been created using a similar procedure. This model is based on the five-shell C₆₀@C₂₄₀@C₅₄₀@C₉₆₀@C₁₅₀₀ concentric fullerene particle. However, in contrast to the type I models, here one single large cavity has been created inside the soot ball in the following way. A second shell atom has randomly been chosen as the center of the initial cavity, and all carbon

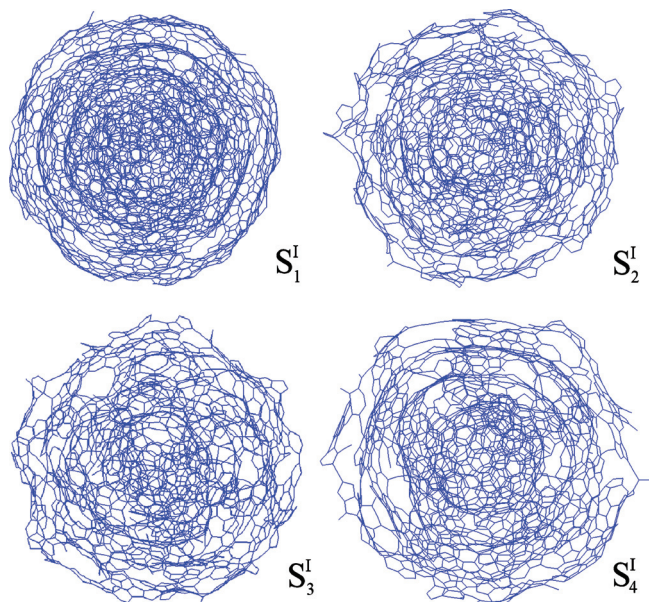


FIG. 1. The four type I soot models: S_1^I , S_2^I , S_3^I , and S_4^I , containing 2976, 2376, 2207, and 2133 atoms, respectively.

atoms that are located within 8.81 Å from this central atom have been removed. The resulting structure has been relaxed in a molecular dynamics simulation with the use of the AIREBO potential in the same way as in the case of the type I soot models. This structure, containing one large cavity is denoted by S^{II} . Finally, to study also the effect of chemical defects on water adsorption a modified version of the S^{II} soot model has also been considered. In our former work we demonstrated that a carbonaceous surface consisting also of several COOH groups can attract more water molecules than the pure carbon surface, whereas the presence of the OH groups has no such effect.³⁷ Therefore, in the modified versions of the S^{II} soot particle the innermost carbon motive (i.e., what remained from the innermost C_{60} fullerene after the removal of the carbon atoms upon creating the cavity) has been substituted with a $C_{19}HCOOH$ unit, consisting of five fused benzene rings (C_{19}) as well as an additional COOH group and a H atom anchored to the surface. The COOH group and the H atom have been placed to the C8 and C9 carbon atoms of this unit, respectively, breaking a double bond of the conjugate system. The resulting C_{19} -COOH unit has then been optimized in *ab initio* calculation.^{29,30} The atomistic structure of this unit as well as the numbering scheme of its carbon atoms is illustrated in Fig. 2. The soot ball obtained by substituting the innermost carbon motive of S^{II} with this $C_{19}HCOOH$ unit

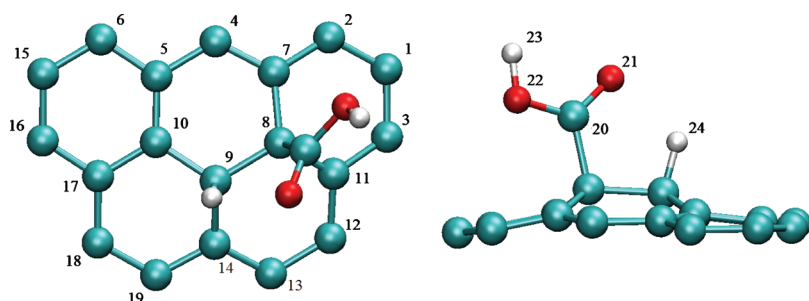


FIG. 2. The $C_{19}HCOOH$ unit placed inside the type II soot model. The numbering of the atoms of this motive is also indicated.

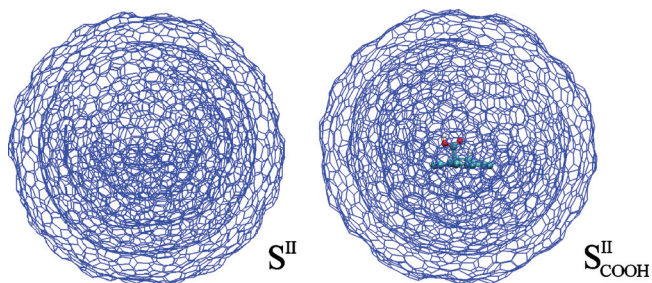


FIG. 3. Type II soot models with and without the $C_{19}HCOOH$ unit inside: S^{II} and S_{COOH}^{II} , both containing 2999 carbon atoms.

is referred to here as S_{COOH}^{II} . The structure of the type II soot particles considered is illustrated in Fig. 3.

The radius of all soot models considered here falls in the range of 17–18 Å. It should finally be emphasized that these models are more realistic representations of soot emitted by aircrafts or collected in flames than what was used in previous studies^{36,37} in the sense that they are chemically stable. Indeed, the soot models considered in former analyses contained randomly distributed carbonaceous units on concentric spheres in a nonoptimized arrangement. In contrast, the stability of the present models is provided by the use of the reactive potential in the relaxation procedure, at least for the soots that are not filled by adsorbed water. Further, the used soot models are also in accordance with the findings of recent electron microscopy measurements.⁴²

B. GCMC simulations

In order to calculate the adsorption isotherm of water on the various soot models, series of Monte Carlo simulations have been performed on the grand canonical (μ, V, T) ensemble at 298 K. The edge length of the basic cubic simulation box has been set to 85.27 Å in every case. Standard periodic boundary conditions have been applied. The value of the chemical potential has been controlled through the B parameter of Adams⁴³

$$\mu = k_B T \left(B + \ln \frac{\Lambda^3}{V} \right), \quad (1)$$

where T is the absolute temperature, V is the volume of the system, k_B is the Boltzmann constant, and Λ is the thermal de Broglie wavelength of water

TABLE I. Lennard-Jones parameters corresponding to the different soot atoms. The numbering scheme of the atoms of the $C_{19}HCOOH$ unit is shown in Fig. 2.

Atom type	Involved atoms	ϵ (kJ mol ⁻¹)	σ (Å)
Hydroxylic O	O22	0.879	2.95
Carbonyl O	O21	0.707	2.99
Carboxylic C	C20	0.439	3.74
C(-COOH)	C8	0.439	3.74
C(-H)	C9	0.439	3.74
Bare C	All other soot atoms	0.273	3.40

$$\Lambda = \frac{h}{\sqrt{2\pi k_B T m}}. \quad (2)$$

Here h is the Planck constant and m is the mass of the water molecule. The simulations have been performed at different B values, ranging between -2 and 1.4 , corresponding to the chemical potential range of -48.5 – -40.1 kJ/mol.

Water molecules have been described by the rigid four-site TIP4P model.⁴⁴ The interaction potential between the soot and the water molecules has been calculated as the sum of pairwise additive atom-atom Lennard-Jones contributions between the atoms of the soot and of the water molecules. A second, electrostatic term of the interaction potential was also taken into account coming from the interaction between point charges located on water molecules and on the $C_{19}HCOOH$ unit. The charges of this latter were computed in *ab initio* calculations.^{29,30} The parameters of these interactions are summarized in Tables I and II.

The soot particles have been regarded as indeformable rigid bodies in the simulations. Moreover, the soot particles have been considered as being chemically inert with respect to water, i.e., water chemisorption or dissociation events have been disregarded. Obviously, these are limitations of the model used, as the soot particle itself might change its geometry due to the adsorbed water molecules, and the possibility of the chemisorption of a few water molecules cannot be excluded either. However, taking these effects into account the AIREBO potential library has to be improved, as carbon-water and water-water interactions have to be included. Work in this direction is currently in progress. All interactions beyond the cut-off radius of 12.5 Å have been truncated to zero. For performing the simulations, Mezei's MMC code⁴⁵ was used. During the simulations water displacement and insertion/deletion attempts have been done in an alternating order. In a particle displacement step a randomly chosen water molecule has been translated to a random distance by no more than 0.25 Å, and rotated around a randomly chosen space-fixed axis by no more than 15° . In an insertion/deletion step either, by 0.5 probability, a randomly chosen water molecule has been tried to be removed from, or, by 0.5 probability, an additional water molecule has been tried to be added to the system. For inserting a molecule the cavity-biased algorithm of Mezei^{46,47} has been applied. The systems have been equilibrated by performing 6×10^8 Monte Carlo steps. In the production stage, the total number of water molecules in the system has been averaged over 4×10^8

TABLE II. Point charges located on the $C_{19}HCOOH$ unit, used in the calculation of the electrostatic interaction between water and soot. The numbering scheme of the atoms is shown in Fig. 2.

Atom	$q(e)$
C(1)	0.026 32
C(2)	-0.007 99
C(3)	-0.038 00
C(4)	-0.015 32
C(5)	-0.057 13
C(6)	0.00000
C(7)	-0.066 14
C(8)	0.147 31
C(9)	0.030 61
C(10)	0.019 69
C(11)	-0.024 32
C(12)	-0.063 98
C(13)	-0.029 78
C(14)	-0.042 32
C(15)	0.000 00
C(16)	0.000 00
C(17)	-0.079 94
C(18)	0.089 44
C(19)	-0.038 08
C(20)	0.709 94
O(21)	-0.504 09
O(22)	-0.588 18
H(23)	0.452 65
H(24)	0.079 31

Monte Carlo steps long trajectories. For further analyses, 4000 equilibrium sample configurations, separated by 10^5 Monte Carlo steps each, have been saved at selected chemical potential values (see Tables III and IV).

III. RESULTS

A. Adsorption isotherms

The adsorption isotherms obtained for the different I and II type soot models are shown in Figs. 4 and 5, respectively, whereas the corresponding numerical data are collected in Tables III and IV, respectively. We have also calculated the desorption branch of the isotherm on the S'_2 soot particle, however, it was found to be practically indistinguishable from the adsorption branch, presumably because of the small size of the pore inside the soot. This result is also consistent with the experimental finding of Kaneko *et al.*,⁴⁸ obtained for carbon aerogels that no adsorption hysteresis occurs in small carbon nanopores. Therefore, we disregard the effect of adsorption hysteresis throughout this paper.

As it is seen from Fig. 4, the different type I model soot particles have rather similar adsorption abilities. Although the adsorption isotherms start to be different from zero at slightly different chemical potentials (i.e., at slightly different pressures), they exhibit a similar, plateau-like part of rather small slope in the chemical potential range preceding condensation. To distinguish between the water molecules adsorbed by the soot particles and the ones being in the vapor phase of the system, we have calculated the average number of water molecules that are located inside the soot

TABLE III. Data of the adsorption isotherms of water on our type I soot particles, as obtained from the simulations. The term “Cond.” indicates the presence of condensed water. The chemical potential values at which sample configurations have been collected for detailed analyses are the same as where the $\langle N_{\text{inside}} \rangle$ value has been evaluated.

B	μ (kJ mol ⁻¹)	S_1^I		S_2^I		S_3^I		S_4^I	
		$\langle N \rangle$	$\langle N_{\text{inside}} \rangle$						
1.40	-40.11			Cond.					
1.30	-40.35			26.09	22.26	Cond.		Cond.	
1.20	-40.60	Cond.		25.69		24.60	20.81	24.96	
1.10	-40.85	24.44							
1.00	-41.09	23.81	19.73	24.21		23.15		23.54	20.20
0.80	-41.59	22.74		22.89		22.10		22.44	
0.50	-42.33	21.36		21.46		20.39		20.24	
0.30	-42.82	20.94		20.31		19.81		19.71	
0.00	-43.56	18.76		19.01		18.12		18.01	
-0.30	-44.30	18.55		16.30		16.91		16.16	14.58
-0.50	-44.79	17.47		15.99	11.61	14.98	14.17	13.31	12.65
-0.65	-45.16					11.68			
-0.80	-45.53	15.03	11.41	1.38		6.55	5.60	3.68	3.50
-1.00	-46.03	5.74	0.72	1.30		2.62		2.04	0.042
-1.20	-46.52	1.31		1.22	0.064	1.56	1.39	1.60	
-1.50	-47.26	1.12		1.11		1.24		1.29	
-2.00	-48.50	1.00		1.00		1.06		1.06	

particle, $\langle N_{\text{inside}} \rangle$, at selected chemical potentials. The obtained values of $\langle N_{\text{inside}} \rangle$ are also included in Tables III and IV and in Figs. 4 and 5. As is seen, all type I soot particles can incorporate about 20 water molecules. In interpreting this result, it should be noted that the largest pore inside these soot models is located in the middle of the particle, inside the innermost fullerene layer, where a C₆₀ fullerene layer could still have been incorporated. The obtained results suggest that the smaller pores scattered inside the different type I soot particles in different densities and in different ways do not play an important role in water adsorption.

This picture is further refined by considering the results obtained for the two type II soot models. As is seen from Fig.

5, the addition of an internal COOH group has a strong effect on the adsorption properties. Namely, the adsorption of water starts at considerably lower chemical potential values (and, hence, at lower vapor pressures) if the adsorbing soot particle contains also a polar COOH group in its internal core. In this case, the water molecules directly bound to the single COOH group can act as a condensation center. Thus, their presence in the system at lower chemical potential values than what corresponds to the appearance of the first water molecules in the bare carbon soot S^{II} attracts also a number of other water molecules, which are bound to these “primary” waters by hydrogen bonding interactions. It is also seen that the saturation plateau of the two isotherms almost perfectly coin-

TABLE IV. Data of the adsorption isotherms of water on our type II soot particles, as obtained from the simulations. The term “Cond.” indicates the presence of condensed water. The chemical potential values at which sample configurations have been collected for detailed analyses are the same as where the $\langle N_{\text{inside}} \rangle$ value has been evaluated.

B	μ (kJ mol ⁻¹)	S^{II}		$S^{\text{II}}_{\text{COOH}}$	
		$\langle N \rangle$	$\langle N_{\text{inside}} \rangle$	$\langle N \rangle$	$\langle N_{\text{inside}} \rangle$
1.20	-40.57	Cond.			
1.10	-40.82	70.63			
1.00	-41.07	70.35	67.52		
0.90	-41.31			Cond.	
0.80	-41.56	68.05		66.73	64.34
0.60	-42.06	66.28		65.74	
0.40	-42.55	63.33	62.18	63.14	
0.30	-42.80	2.49		62.89	
0.20	-43.04	2.30	1.052	62.03	
0.00	-43.54	2.04		59.09	56.48
-0.10	-43.78			57.74	
-0.20	-44.03	1.82		4.19	2.32
-0.40	-44.52			3.25	
-0.60	-45.02			2.83	

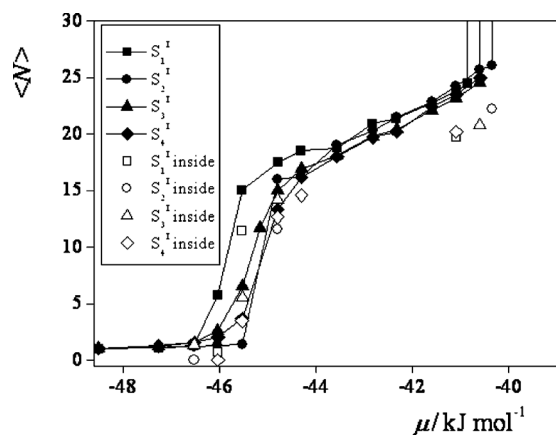


FIG. 4. The adsorption isotherms obtained on type I soot models: S_1^I (squares), S_2^I (circles), S_3^I (triangles), and S_4^I (diamonds). Open circles correspond to the equilibrium number of water molecules inside the soot particles.

cides with each other, both of the type II soots considered can incorporate about 65–70 water molecules, reflecting also the much larger size of this pore than that in the type I soot particles.

The obtained results suggest that two possible factors might determine the adsorption ability of the different soot particles. First, the size and shape of the pore plays an important role in this respect. It is clear that the main driving force of water adsorption in large apolar carriers, such as soot balls is the water-water interaction, i.e., the possibility of hydrogen bond formation with already adsorbed water molecules.^{36,37} Therefore, adsorbing pores should be large enough, and their shape should be sufficiently compact to host a large enough water cluster the molecules of which can form a sufficient number of hydrogen bonds to stabilize themselves in the apolar environment. If the pore is too small or it is simply too narrow then the number of hydrogen bonded neighbors of the water molecules is limited by these geometric constraints. In this case, the energy gain of the adsorbed water molecules might not overcompensate the effect of the entropy loss accompanying their clustering, which prevents their adsorption. This seems to be the case in the smaller pores of the type I soot particles. It should be noted

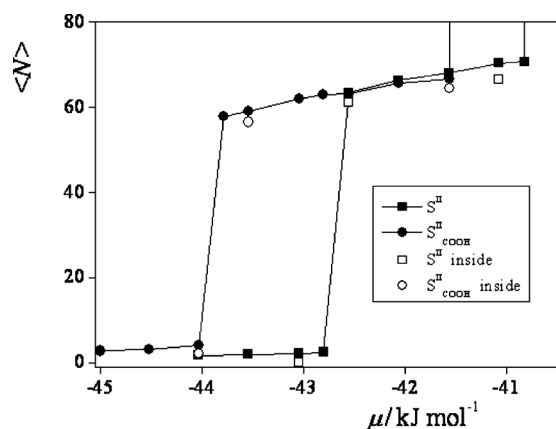


FIG. 5. Adsorption isotherms obtained on type II soot models: S^{II} (squares) and S_{COOH}^{II} (circles). Open symbols indicate the average number of waters inside the soot particles.

that similar behavior was found by Striolo *et al.*⁴⁹ for water in carbon nanotubes containing oxygenated sites. Further, the amount of water a soot particle can adsorb is obviously related to the size of the pore inside the soot.

On the other hand, water-water interaction can only lead to the adsorption of new water molecules if the soot already contains at least some traces of water. Thus, the second possible factor that might determine adsorption is the ability of the soot particle of attracting the first few water molecules. In other words, the pores inside the soot might contain a few adsorption sites at which water molecules can be particularly strongly bound even in the absence of other water molecules. In this case, these first adsorbed waters can act as nucleation centers for the adsorption at higher chemical potential values. This effect is clearly demonstrated in the case of the type II soot particles, where the optimal location of the first adsorbed water molecules can indeed initiate the adsorption of other water molecules, and it is also likely the factor responsible for the fact that the adsorption isotherms obtained on the different type I soot particles start at different chemical potentials.

In order to investigate the role of these two factors, i.e., that of the optimal location of the first adsorbed molecules and of the optimal pore shape, in the following we analyze in detail the position of the first adsorbed molecules inside the various soot balls, the morphological properties of the pores in our various soot models, and the energetic background of the adsorption process investigated.

B. Position of the first adsorbed molecules

In order to investigate the role of the position of the first few adsorbed water molecules we have determined the position of the water molecules inside the S_2^I , S_3^I , and S_{COOH}^{II} soot balls at very low loadings, i.e., at the chemical potential values of -46.52 kJ/mol (S_2^I and S_3^I) and -44.03 kJ/mol (S_{COOH}^{II}). In these systems the S_2^I , S_3^I , and S_{COOH}^{II} soots contain, on average, 0.064, 1.4, and 2.32 water molecules, respectively (see Tables III and IV). To map the position of the adsorbed water molecules, we set a $120 \times 120 \times 120$ grid on each soot (using the grid spacing of 0.33 Å) and marked the grid points at which an adsorbed water molecule is found at least ν times in our samples. The value of ν is set to 1, 3, and 10 for the S_2^I , S_3^I , and S_{COOH}^{II} soot balls, respectively.

The maps of these first adsorbed water molecules inside the S_2^I , S_3^I , and S_{COOH}^{II} soots are shown in Fig. 6. As is seen, in all cases there are some particular regions of the largest, innermost cavity where these water molecules prefer to stay. When looking at the preferred locations of the first adsorbed water molecules inside the S_3^I soot [Fig. 6(b)] it is seen that there are only a few positions where they can bind at low pressures. These binding positions are located close to the surface of the pores at points where it is locally of rather large curvature, and hence a large number of close water-carbon contacts can be formed. Such positions are typically located at the vicinity of a pentagonal face of the fullerene layer (as the curvature of the fullerene surface is larger around the pentagonal than around the hexagonal faces). Such a “nest” for an initially adsorbed water molecule is

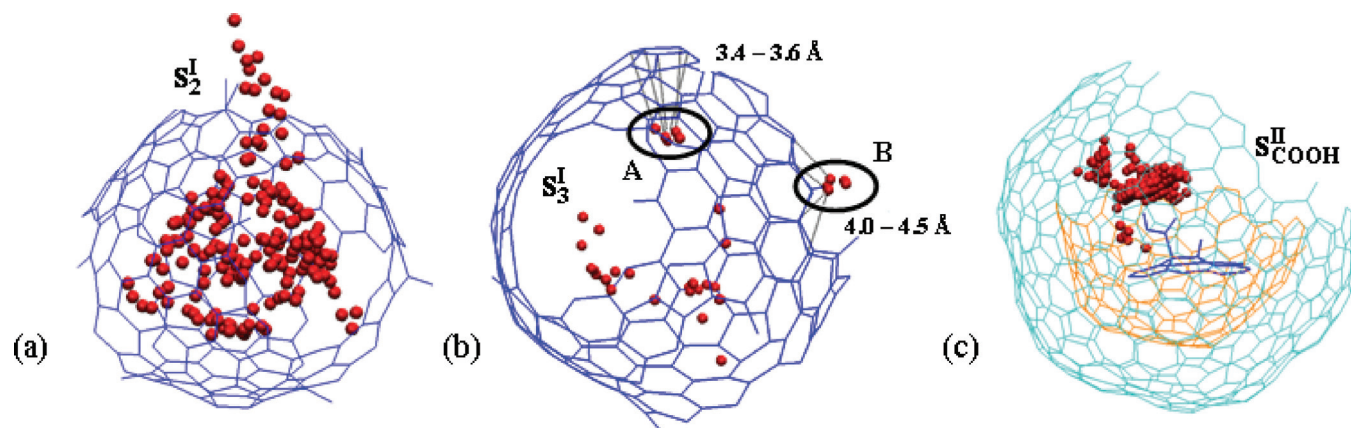


FIG. 6. Preferential positions of the first adsorbed water molecules inside (a) the S_2^I , (b) the S_3^I , and (c) the $S_{\text{COOH}}^{\text{II}}$ soot ball at low loading. For clarity, only the inner part of the soot balls is shown.

marked by A in Fig. 6(b). As is seen, in this position the distance of the adsorbed water molecule from all the C atoms of the nearby pentagonal face falls always between 3.4 and 3.6 Å. Another possibility is if the water molecule is close to the C atoms of two consecutive fullerene layers. An example for this is the position marked by B in Fig. 6(b), which is located in a small pore, merged with the largest cavity inside the soot. In this way, the water molecule occupying position B can be equally close (i.e., within 4.0–4.5 Å) to a number of C atoms of the innermost fullerene layer and also to those of the outer layer [not shown in Fig. 6(b) for clarity].

In order to emphasize the important role played by the first adsorbed water molecules in the adsorption process we have calculated the isosteric heat of water adsorption, H^{ads} , in the four type I soot models considered at very low loadings, according to the fluctuation formula⁵⁰

$$H^{\text{ads}} = RT - \frac{\langle UN_{\text{inside}} \rangle - \langle U \rangle \langle N_{\text{inside}} \rangle}{\langle N_{\text{inside}}^2 \rangle - \langle N_{\text{inside}} \rangle^2}, \quad (3)$$

where the angled brackets $\langle \dots \rangle$ denote ensemble averaging, U stands for the potential energy of the system, and R is the gas constant. The obtained isosteric heat of adsorption data along with the corresponding $\langle N_{\text{inside}} \rangle$ values are collected in Table V. As is seen, the value of H^{ads} is already rather close to the heat of evaporation of the TIP4P water model of 44.6 kJ/mol (Ref. 44) if the average number of adsorbed water molecules is around 1, and differs considerably from this value only if the average number of adsorbed waters is about an order of magnitude smaller.

Finally, Fig. 6(c) shows the preferential location of the first water molecules adsorbed by the $S_{\text{COOH}}^{\text{II}}$ soot. As is expected, these water molecules are almost exclusively located around the polar COOH group of the $\text{C}_{19}\text{HCOOH}$ unit, presumably forming multiple hydrogen bonds with it.

TABLE V. Isosteric heat of adsorption of water in the different pure carbon soot models considered at low coverage.

Soot model	S_1^I	S_2^I	S_3^I	S_4^I
$\langle N_{\text{inside}} \rangle$	0.72	0.064	0.042	1.39
$H^{\text{ads}}(\text{kJ mol}^{-1})$	41.3	16.0	8.2	39.0

C. Analysis of the pore morphology

In order to investigate the role of the second possible factor, i.e., pore morphology on the adsorption ability of the soot ball, we analyze here the size, the length, and the volume of the pores in our soot models. (It should be recalled that although the pores have originally been created by removing the C atoms located within a predefined sphere from the soot ball, this initial spherical shape of the pores might have been severely modified during the relaxation of the soot particles in the molecular dynamics simulations done with the reactive AIREBO potential, see Sec. II A).

A very efficient approach of studying the morphology of interatomic pores is based on the Voronoi–Delaunay method.^{51–55} In a three dimensional assembly of atoms, the Voronoi region of a given atom is the locus of the spatial points that are closer to this atom than to any other one. If all the atoms are of the same size, this region is the well known Voronoi polyhedron.^{56,57} If the assembly consists of atoms of different radii, the edges and faces of the Voronoi regions are curved.^{58,59} In any case, the Voronoi regions constructed for all atoms constitute a tessellation, i.e., a decomposition of space without gaps and overlaps. The edges and vertices of the Voronoi regions constitute a network, called the Voronoi network. Vertices of this network are the centers of the largest inscribed empty spheres (spherical voids) between quadruplets of four mutually neighboring atoms. Such quadruplets of atoms determine the Delaunay simplexes and represent the simplest cavities located between the atoms. Any complex pore can be regarded as a cluster of such simplexes, and the empty space inside the pore can be represented as a union of the inscribed empty spheres. Further, edges of the Voronoi network represent fairways passing through the narrow bottlenecks between three atoms from one vertex to the neighboring one. These features make the Voronoi network a very convenient tool for pore analysis, since having this network calculated the properties of the corresponding pores can easily be calculated.^{53,54}

Algorithms and programs for constructing the Voronoi network can easily be found in the literature for the special case of uniform atom size.⁶⁰ For constructing the Voronoi network in the general case of atoms of different radii, we

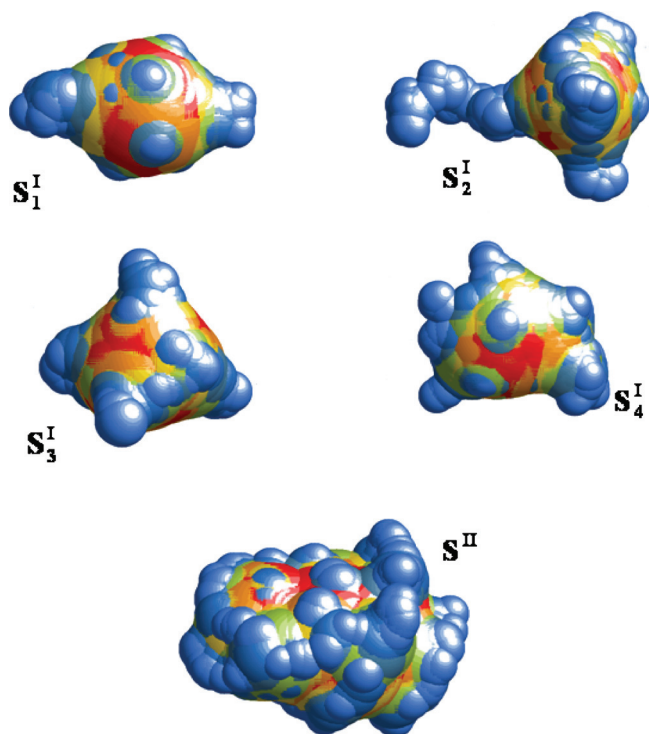


FIG. 7. Representation of the largest voids, shown as the union of simplicial spherical cavities inside the five different bare carbon soots considered. Different colors correspond to spheres of different radii.

recently proposed an efficient algorithm.⁶¹ Note that our soot models consist of only C atoms of uniform size, with the exception of the O atoms of the $C_{19}HCOOH$ unit present in the S_{COOH}^{II} soot model. (Since H atoms do not carry Lennard-Jones interaction centers, they are neglected in this analysis.)

A physically meaningful way of defining pores is to regard regions of the empty interatomic space that are accessible for a spherical probe of the predefined radius R_{probe} . Here we set R_{probe} to be 1.4 \AA , corresponding roughly to the size of a water O atom. In this way, regions of the empty space between the soot C atoms that are accessible for a single water molecule are considered as pores. Thus, interstitial spheres (determined by the Delaunay simplexes) with the radius larger than 1.4 \AA correspond to the simplicial cavities accessible for our probe. Further, if the bottleneck radius between two such neighboring simplicial cavities is also larger than 1.4 \AA , both of them are included in the same cluster, and hence belong to the same complex pore. In this way, all the pores accessible for a water molecule can be detected. Such a pore can be described as an aggregate of the (usually strongly overlapping) interstitial spheres. The largest pores inside the five bare carbon soot models considered are shown in Fig. 7 as assemblies of empty spheres with radii of at least 1.4 \AA (the pore inside the S_{COOH}^{II} soot particle is not shown, since it looks almost indistinguishable from that in the S^{II} particle).

In analyzing the morphology of the interatomic pores in our soot models we have calculated the following characteristics. The volume of a pore V is calculated as the sum of the empty volume of the corresponding Delaunay simplexes. Pores can also be characterized by the radius of the largest simplicial cavity belonging to them, R_{max} , and by their length

TABLE VI. Properties of the largest pores in the different soot models considered.

Soot model	V (\AA^3)	L (\AA)	R_{max} (\AA)	N_{sp}	N_{max}	$\langle N \rangle_{ads}$
S_1^I	803	18.5	4.89	16.3	26.8	19.7
S_2^I	1132	22.4	4.73	14.8	37.8	22.8
S_3^I	869	15.6	4.69	14.4	29.0	20.8
S_4^I	868	17.6	4.48	12.6	29.0	20.2
S^{II}	2497	22.2	5.23	20.0	83.4	66.5
S_{COOH}^{II}	2478	22.2	5.15	19.1	82.8	64.3

(i.e., the largest distance between two points inside the corresponding aggregate of simplicial cavities), L . In the pore morphology analysis we take only the largest pore into account in each of the six soot particles considered.

The values of V , R_{max} , and L corresponding to the different soot models are summarized in Table VI. This table also contains the maximum number of water molecules that could be incorporated in the largest pore and in the largest spherical cavity, N_{max} and N_{sp} , respectively (calculated assuming the experimental number density of liquid water of 0.0334 \AA^{-3}), and the average number of water molecules found to be adsorbed inside the soot at the highest loading, $\langle N \rangle_{ads}$. As is seen, the pores can, on one hand, always incorporate considerably more water molecules than what would correspond to the volume of their largest simplicial spherical cavity, but, on the other hand, they never contain as much water as what would correspond to their total volume. Instead, even at the highest loading the water content of these pores is just 60%–80% of their nominal capacity. These findings suggest that (i) the water content of the smaller pores is negligible (as even the largest pore is never completely filled, and the saturation part of the isotherms corresponding to soots of different densities of the small cavities agrees well with each other, see Fig. 4), and (ii) similarly to the pores themselves, the shape of the water droplets located inside them is also highly nonspherical (as the water clusters located inside the pores are considerable larger than the largest spherical clusters that could fit into the pores). However, the shape of the water droplet does not necessarily follow strictly that of the pore, as reflected in the difference of the $\langle N \rangle_{ads}$ and N_{max} values. Since the main driving force of the water adsorption on soot is shown to be the possibility of the formation of new water-water hydrogen bonds, the shape of the water droplet (and hence the number of the water molecules belonging to it) is determined by the requirement that, within the constraints imposed by the pore shape, the hydrogen bonding network of the adsorbed water molecules should be optimal (i.e., the number of hydrogen bonded neighbors of the water molecules should be as much as possible). In particular, narrow and elongated pockets of the pore, where the hydrogen bonding ability of the water molecules is strongly limited by steric factors, are likely not to be completely filled even up to the point of condensation.

This requirement also implies that the more spherical a pore is the more efficiently it can be filled. In order to demonstrate this, we have calculated the value of $\langle N \rangle_{ads}/N_{max}$,

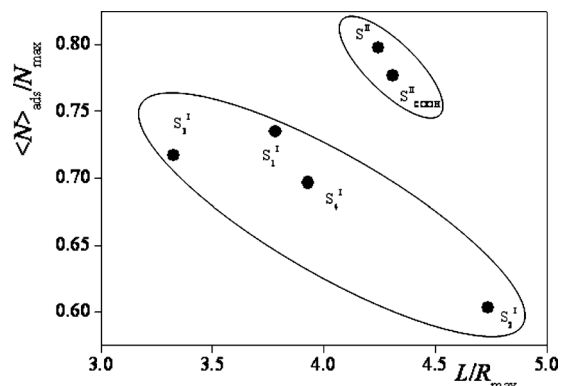


FIG. 8. Ratio of the average number of water molecules found to be adsorbed inside the soot at the highest loading, $\langle N \rangle_{\text{ads}}$, and the maximum number of water molecules that could be incorporated in the largest pore of the soot, N_{max} , as a function of the ratio of the length of the largest pore and the radius of the largest interstitial sphere inside it, L/R_{max} . Points corresponding to similar (i.e., type I or type II) soot particles are encircled in order to emphasize the observed trend for similar pores.

characterizing the relative filling of the pores, as a function of the ratio of L/R_{max} (i.e., that of the linear size of the pore and the radius of its largest spherical cavity), characterizing the deviation of the pore shape from the perfect sphere. The obtained data are shown in Fig. 8. The correlation between $\langle N \rangle_{\text{ads}}/N_{\text{max}}$ and L/R_{max} is clear for both types of soot, indicating that, at least in the case of not too much different pores, more spherical pores can more efficiently be filled by the adsorbed water molecules.

D. Energetics of the adsorption

In order to investigate the energetic background of the adsorption in detail we have also calculated the distribution of the binding energy of the adsorbed water molecules, U_b (i.e., their interaction energy with the rest of the system) as well as its contributions coming from the interaction with the soot ball and with the other water molecules, U_b^{soot} and U_b^{wat} , respectively, for all the six soot particles considered both at low and at high loading. To avoid the effect of the water molecules being in the vapor phase around the soot ball, we have only taken into account the water molecules located inside the soot in this analysis. The obtained $P(U_b)$, $P(U_b^{\text{soot}})$, and $P(U_b^{\text{wat}})$ distributions are shown in Figs. 9 and 10 for the type I and II soots, respectively.

In the case of low loadings some water molecules are found to be isolated from each other as well as from the soot ball, as reflected in the high and narrow peak of the $P(U_b)$, $P(U_b^{\text{soot}})$, and $P(U_b^{\text{wat}})$ distributions at zero energy. These molecules, although being inside the soot, are clearly in the vapor phase, which is also present inside large pores of the soot at low loadings. In the case of the bare carbon soots, the energy of interaction of the adsorbed water molecules with the soot ball turns out to be around -10 kJ/mol. In the case of the S_1^I soot ball the peak of the $P(U_b^{\text{soot}})$ distribution is located at somewhat lower energies (i.e., around -11 kJ/mol) than for the other type I soots, where this value is always around -8.5 kJ/mol [see the inset of Fig. 9(a)]. This difference is in accordance with our previous finding that adsorption on the S_1^I soot starts at somewhat lower

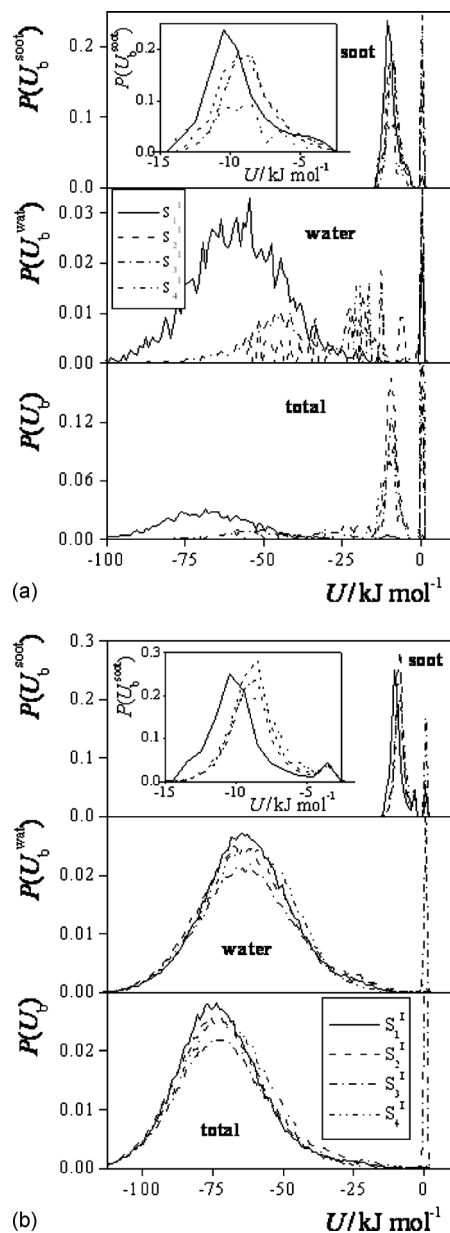


FIG. 9. Distributions of the total binding energy of the water molecules (U_b , bottom panel) and of the contributions coming from the interaction with the other water molecules (U_b^{wat} , middle panel) and with the soot ball (U_b^{soot} , top panel) in the case of the S_1^I (full line), S_2^I (dashed line), S_3^I (dash-dotted line), and S_4^I (dash-dot-dotted line) soot at (a) low and (b) high loading. The inset shows the low energy part of the $P(U_b)$ curves on a magnified scale.

chemical potentials (pressures) than that on the other type I soot balls (see Fig. 4), and stresses again the role of the optimal location of the first adsorbed water molecules in the adsorption process. It should also be noted that among the type I soots S_1^I contains far the largest number of C atoms, which is likely to be related with its ability of more easily binding the first few water molecules than the other type I soots.

It is also seen from Fig. 9(a) that in the case of the S_1^I and S_3^I soots, which contain a much larger amount of water at the selected chemical potential than either S_2^I or S_4^I , the $P(U_b^{\text{soot}})$ distribution already exhibits a shoulder at its high energy side, around -5 kJ/mol. This shoulder reflects the presence of water molecules that are weakly bound to the

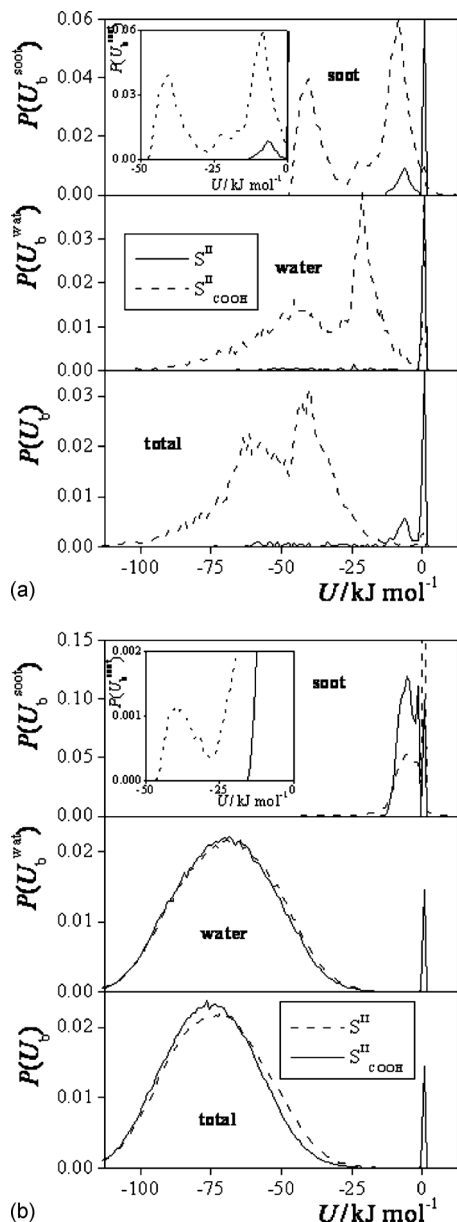


FIG. 10. Distributions of the total binding energy of the water molecules (U_b , bottom panel) and of the contributions coming from the interaction with the other water molecules (U_b^{wat} , middle panel) and with the soot ball (U_b^{soot} , top panel) in the case of the S^{II} (full line) and $S^{\text{II}}_{\text{COOH}}$ (dashed line) soot at (a) low and (b) high loading. The inset shows the low energy part of the $P(U_b)$ curves on a magnified scale.

soot, as they are already bound by the other adsorbed water molecules rather than by the soot ball itself. Correspondingly, the $P(U_b^{\text{wat}})$ distribution of these soots show a peak around -20 kJ mol^{-1} and another one between -45 and -60 kJ mol^{-1} . The former peak corresponds to waters with one, whereas the latter one to waters with two or three hydrogen bonded neighbors. It should also be noted that traces of the peak around -20 kJ mol^{-1} already appear on the $P(U_b^{\text{wat}})$ distribution of the S^{I} soot, clearly demonstrating that the main driving force of the water adsorption on soot is the possibility of the formation of new water-water hydrogen bonds with the already adsorbed water molecules.

The $P(U_b^{\text{soot}})$ distributions of the type I soots obtained at high loading [Fig. 9(b)] are rather similar to those corre-

sponding to low loading. It should be noted that now the majority (i.e., about 80–90%) of the water molecules have interaction energy of roughly -10 kJ mol^{-1} with the soot ball. This finding reflects the relatively small size of the largest pore of these soot balls, as even at high loading the majority of the adsorbed water molecules is still in contact with the wall of the pore. The $P(U_b^{\text{wat}})$ distribution exhibits a single, broad peak around -63 kJ mol^{-1} , indicating that the adsorbed water molecules form, on average, three hydrogen bonds with each other. The peak of the total binding energy distribution appears at -72 kJ mol^{-1} , which agrees almost perfectly with the sum of the peak positions of the $P(U_b^{\text{soot}})$ and $P(U_b^{\text{wat}})$ distributions.

The distributions corresponding to the bare carbon S^{II} soot ball show rather similar characteristics to those of the type I soots. At low loading [Fig. 10(a)] the interaction energy of the adsorbed water molecules with the soot ball has a peak at about -6.5 kJ mol^{-1} , reflecting the larger size of this pore, and hence the smaller curvature of its wall than that of the pores in the type I soots. The $P(U_b^{\text{wat}})$ distribution shows traces of a broad and flat peak between -20 and -50 kJ mol^{-1} , corresponding to the few water molecules with one or two hydrogen bonded neighbors.

In the case of the $S^{\text{II}}_{\text{COOH}}$ soot, however, the picture is rather different, at least at low loading [Fig. 10(a)]. Here the $P(U_b^{\text{soot}})$ distribution is bimodal, having a peak at -40 kJ mol^{-1} and another one at -8 kJ mol^{-1} . The first peak reflects the water molecules double hydrogen bonded to the COOH group, whereas the second peak corresponds to water molecules forming no hydrogen bond with this group, but interacting with the nearby C atoms of the pore wall. These waters are already hydrogen bonded to other waters, as reflected in the peaks of the $P(U_b^{\text{wat}})$ distribution at -21 and -45 kJ mol^{-1} , given by waters with one and with two hydrogen bonded water neighbors, respectively. The peaks of the $P(U_b)$ total binding energy distribution, appearing around -60 and -40 kJ mol^{-1} indicate that the adsorbed water molecules form either two or three hydrogen bonds with their neighbors. In the light of our previous finding we can conclude that in the former case both hydrogen bonds are typically formed with another water molecule, whereas in the latter case two hydrogen bonds are formed with the COOH group and the third one with a water molecule.

The differences between the bare carbon S^{II} and the COOH-containing $S^{\text{II}}_{\text{COOH}}$ soots, however, disappear at high loading [see Fig. 10(b)], in accordance with our previous finding that the role of the polar COOH group is limited to the initiation of the adsorption at low pressures. Here the amplitude of the peak of the $P(U_b^{\text{soot}})$ distribution of the $S^{\text{II}}_{\text{COOH}}$ soot at -40 kJ mol^{-1} is an order of magnitude smaller than that at low loading [see the inset of Fig. 10(b)], as hydrogen bonding with the COOH group now involves only a small minority of the adsorbed water molecules. Further, the majority of the waters (although not such a large fraction as in the case of the type I soots) are still in contact with the pore wall, and they form, on average, three hydrogen bonds with each other, irrespective of whether the soot contains a polar COOH group or not.

IV. SUMMARY AND CONCLUSIONS

In this paper we have investigated the adsorption process of water on model soot particles by means of the GCMC method, and related the characteristics of the pores inside the soot ball with their adsorption ability. To the best of our knowledge, this is the first time when such a study is performed on chemically stable models of soot.

The obtained results clearly show that the main driving force of water adsorption on soot is the possibility of the formation of new water-water hydrogen bonds with the already adsorbed water molecules. We found that there are two important factors influencing the adsorption ability of soot. The first of these factors is the ability of the soot of accommodating the first adsorbed water molecules. Since the presence of these molecules initiates the adsorption of other waters, the stronger these first water molecules can be bound by the soot, the earlier the adsorption starts. This can be achieved when strong hydrophilic sites are present in the soot.

The other factor concerns morphological characteristics, primarily size and shape of the pores. In general, adsorbing pores should be such that the hydrogen bonding network of the water molecules filling them should be optimal. It turned out that this requirement practically means that water molecules should be able of forming, on average, three hydrogen bonds with each other. This implies that too small pores as well as narrow and deep pockets of the larger pores are not filled with water even at high pressures. Although the adsorbed water droplet is found not to be spherical, it turned out that, in general, more spherical pores can be more efficiently filled with water at high loading.

It is also clear that the size of the pores or, in other words, the density of the soot is a crucial factor of the adsorption. Thus, smaller pores meet better with the first criterion, as the first adsorbed water molecules can interact stronger with the nearby C atoms of the soot in a small pore of highly curved wall. On the other hand, such pores satisfy less the second criterion, as the hydrogen bonding network of water filling smaller pores is more strongly restricted by steric factors. In accordance with former experimental findings,⁴⁸ our results thus suggest that there might be an optimal range of pore sizes in soots which corresponds to the best water adsorption ability of the soot, i.e., when it is able to bind a noticeable amount of water even at rather low pressures.

ACKNOWLEDGMENTS

This project is partly supported by the Hungarian OTKA Foundation under project no. 75328, by RFFI Grant No. 8-03-00140, by the Hungarian-French Intergovernmental Science and Technology Program (BALATON) under project no. FR-27/09, and by the MTA-CNRS collaboration programme. G.H.'s Ph.D. is partly granted by the French Government thanks to the program "Bourses du Gouvernement Français." We also thank Mihaly Mezei for fruitful discussions and to Steven Stuart for providing the AIREBO code.

- ¹J. E. Penner, D. H. Lister, D. J. Griggs, D. J. Dokken, and M. McFarland, *Aviation and the Global Atmosphere. Special Report of the Intergovernmental Panel on Climate Change* (Cambridge University Press, Cambridge, 1999), pp. 87–94.
- ²W. Cantrell and A. Heymsfeld, *Bull. Am. Meteorol. Soc.* **86**, 795 (2005).
- ³B. Kärcher, *Surv. Geophys.* **20**, 113 (1999).
- ⁴J. Hendricks, B. Kärcher, A. Döpelheuer, J. Feichter, U. Lohmann, and D. Baumgardner, *Atmos. Chem. Phys.* **4**, 2521 (2004).
- ⁵J. Hendricks, B. Kärcher, U. Lohmann, and M. Ponater, *Geophys. Res. Lett.* **32**, L12814 (2005).
- ⁶M. A. Zondlo, P. K. Hudson, A. J. Prenni, and M. A. Tolbert, *Annu. Rev. Phys. Chem.* **51**, 473 (2000).
- ⁷U. Pöschl, T. Letzel, C. Schauer, and R. Niessner, *J. Phys. Chem. A* **105**, 4029 (2001).
- ⁸D. G. Aubin and J. P. D. Abbatt, *Environ. Sci. Technol.* **40**, 179 (2006).
- ⁹N. O. A. Kwamena, M. E. Earp, C. J. Young, and J. P. D. Abbatt, *J. Phys. Chem. A* **110**, 3638 (2006).
- ¹⁰J. P. D. Abbatt, *Chem. Rev. (Washington, D.C.)* **103**, 4783 (2003).
- ¹¹O. B. Popovicheva and A. Starik, *Atmos. Oceanic Phys.* **43**, 147 (2007).
- ¹²O. B. Popovicheva, N. M. Persiantseva, M. E. Trukhin, G. B. Rulev, N. K. Shonija, Y. Y. Buriko, A. M. Starik, B. Demirdjian, D. Ferry, and J. Suzanne, *Phys. Chem. Chem. Phys.* **2**, 4421 (2000).
- ¹³D. Delhaye, "Experimental determination of physical and chemical characteristics of soot emitted by aircraft engines (in French)," Ph.D. thesis, University of Aix-Marseille II, 2007.
- ¹⁴O. B. Popovicheva, N. M. Persiantseva, B. V. Kuznetsov, N. K. Rakhmanova, N. K. Shonija, J. Suzanne, and D. Ferry, *J. Phys. Chem. A* **107**, 10046 (2003).
- ¹⁵O. B. Popovicheva, M. E. Trukhin, N. M. Persiantseva, and N. K. Shonija, *Atmos. Environ.* **35**, 1673 (2001).
- ¹⁶B. P. T. Kärcher, U. M. Biermann, and U. Schumann, *J. Atmos. Sci.* **53**, 3066 (1996).
- ¹⁷D. Ferry, J. Suzanne, S. Nitsche, O. B. Popovicheva, and N. K. Shonija, *J. Geophys. Res.* **107**, 4734 (2002).
- ¹⁸C. Alcalá-Jorrod, H. van der Bergh, and M. J. Rossi, *Geophys. Res. Lett.* **29**, 1820 (2002).
- ¹⁹A. R. Chughtai, N. J. Miller, D. M. Smith, and J. R. Pitts, *J. Atmos. Chem.* **34**, 259 (1999).
- ²⁰B. Gorbunov, A. Baklanov, N. Kakutkina, H. L. Windsor, and R. Toumi, *J. Aerosol Sci.* **32**, 199 (2001).
- ²¹S. Seisel, A. Pashkova, Y. Lian, and R. Zellner, *Faraday Discuss.* **130**, 437 (2005).
- ²²A. R. Chughtai, J. M. Kim, and D. M. Smith, *J. Atmos. Chem.* **43**, 21 (2002).
- ²³E. A. Müller, L. F. Rull, L. F. Vega, and K. E. Gubbins, *J. Phys. Chem.* **100**, 1189 (1996).
- ²⁴E. A. Müller and K. E. Gubbins, *Carbon* **36**, 1433 (1998).
- ²⁵C. L. McCallum, T. J. Bandosz, S. C. McGrother, E. A. Müller, and K. E. Gubbins, *Langmuir* **15**, 533 (1999).
- ²⁶J. K. Brennan, T. J. Bandosz, K. T. Thomson, and K. E. Gubbins, *Colloids Surf., A* **187–188**, 539 (2001).
- ²⁷M. Jorge, C. Schumacher, and N. A. Seaton, *Langmuir* **18**, 9296 (2002).
- ²⁸A. Striolo, A. A. Chialvo, K. E. Gubbins, and P. T. Cummings, *J. Chem. Phys.* **122**, 234712 (2005).
- ²⁹S. Hamad, J. A. Mejias, S. Lago, S. Picaud, and P. N. M. Hoang, *J. Phys. Chem. B* **108**, 5405 (2004).
- ³⁰B. Collignon, P. N. M. Hoang, S. Picaud, and J. C. Rayez, *Chem. Phys. Lett.* **406**, 430 (2005).
- ³¹B. Collignon, P. N. M. Hoang, S. Picaud, and J. C. Rayez, *Comput. Lett.* **1**, 277 (2005).
- ³²M. Oubal, S. Picaud, M. T. Rayez, and J. C. Rayez, *Carbon* **48**, 1570 (2010).
- ³³S. Picaud, P. N. M. Hoang, S. Hamad, J. A. Mejias, and S. Lago, *J. Phys. Chem. B* **108**, 5410 (2004).
- ³⁴S. Picaud, B. Collignon, P. N. M. Hoang, and J. C. Rayez, *J. Phys. Chem.* **110**, 8398 (2006).
- ³⁵S. Picaud, B. Collignon, P. N. M. Hoang, and J. C. Rayez, *Phys. Chem. Chem. Phys.* **10**, 6998 (2008).
- ³⁶F. Moulin, S. Picaud, P. N. M. Hoang, L. Pártay, and P. Jedlovsky, *Mol. Simul.* **32**, 487 (2006).
- ³⁷F. Moulin, S. Picaud, P. N. M. Hoang, and P. Jedlovsky, *J. Chem. Phys.* **127**, 164719 (2007).
- ³⁸M. P. Allen and D. J. Tildesley, *Computer Simulations of Liquids* (Clarendon, Oxford, 1987).

- ³⁹S. J. Stuart, A. B. Tutein, and J. A. Harrison, *J. Chem. Phys.* **112**, 6472 (2000).
- ⁴⁰D. W. Brenner, O. A. Shenderova, J. A. Harrison, S. J. Stuart, B. Ni, and S. B. Sinnott, *J. Phys.: Condens. Matter* **14**, 783 (2002).
- ⁴¹A. V. Shevade, S. Jiang, and K. E. Gubbins, *Mol. Phys.* **97**, 1139 (1999).
- ⁴²B. Demirdjian, D. Ferry, J. Suzanne, O. B. Popovicheva, N. M. Persian-tseva, and N. K. Shonija, *J. Atmos. Chem.* **56**, 83 (2007).
- ⁴³D. J. Adams, *Mol. Phys.* **29**, 307 (1975).
- ⁴⁴W. L. Jorgensen, J. Chandrasekhar, J. F. Madura, R. W. Impey, and M. L. Klein, *J. Chem. Phys.* **79**, 926 (1983).
- ⁴⁵See <http://fulcrum.physbio.mssm.edu/~mezei/mmc> for MMC program.
- ⁴⁶M. Mezei, *Mol. Phys.* **40**, 901 (1980).
- ⁴⁷M. Mezei, *Mol. Phys.* **61**, 565 (1987); **67**, 1207 (1989).
- ⁴⁸K. Kaneko, Y. Hanzawa, T. Iiyama, T. Kanda, and T. Suzuki, *Adsorption* **5**, 7 (1999).
- ⁴⁹A. Striolo, A. A. Chialvo, P. T. Cummings, and K. E. Gubbins, *J. Chem. Phys.* **124**, 074710 (2006).
- ⁵⁰D. Nicholson and N. G. Parsonage, *Computer Simulation and the Statistical Mechanical Theory of Adsorption* (Academic, London, 1982).
- ⁵¹N. N. Medvedev, in *Voronoi's Impact on Modern Science*, edited by P. Engel and H. Syta (Institute of Mathematics, Kiev, 1998), Vols. 1-2, pp. 164–175.
- ⁵²H. Edelsbrunner, M. A. Facello, and J. Liang, *Discrete Appl. Math.* **88**, 83 (1998).
- ⁵³M. G. Alinchenko, A. V. Anikeenko, N. N. Medvedev, V. P. Voloshin, M. Mezei, and P. Jedlovsky, *J. Phys. Chem. B* **108**, 19056 (2004).
- ⁵⁴M. G. Alinchenko, V. P. Voloshin, N. N. Medvedev, M. Mezei, L. Pártay, and P. Jedlovsky, *J. Phys. Chem. B* **109**, 16490 (2005).
- ⁵⁵G. Malavasi, M. C. Menziani, A. Pedone, and U. Segre, *J. Non-Cryst. Solids* **352**, 285 (2006).
- ⁵⁶G. F. Voronoi, *J. Reine Angew. Math.* **134**, 198 (1908).
- ⁵⁷B. N. Delaunay, Proceedings of the Mathematics Congress, Toronto 11–16 August 1928, Vol. 1924, p. 695.
- ⁵⁸A. Okabe, B. Boots, K. Sugihara, and S. N. Chiu, *Spatial Tessellations: Concepts and Applications of Voronoi Diagrams* (Wiley, Chichester, 2000).
- ⁵⁹N. N. Medvedev, *The Voronoi–Delaunay Method in the Structural Investigation of Non-crystalline Systems* (SB RAS, Novosibirsk, 2000) (in Russian).
- ⁶⁰See <http://www.cgal.org/> for example, a geometric library.
- ⁶¹N. N. Medvedev, V. P. Voloshin, V. A. Luchnikov, and M. L. Gavrilova, *J. Comput. Chem.* **27**, 1676 (2006).